Title no. 96-S110

Use of Fiber-Reinforced Plastics Versus Steel for Shear Reinforcement of Concrete

by Tim Ibell and Chris Burgoyne

The use of fiber-reinforced plastics (FRPs) for the reinforcement of concrete structures is receiving much attention at present. Attempts are being made to better understand the behavior of concrete containing these fibrous materials. Much of this work, however, is aimed at attempting to fit present design guidelines to this wholly new construction material. This paper presents pushoff tests and suggests analytical techniques for the shear capacity of concrete reinforced with FRPs. As a basis for comparison, tests on specimens containing steel stirrups are also presented. It is shown that while plasticity theory may be considered appropriate for use in the steel-reinforced situation, other analysis techniques are required for FRP-reinforced specimens. This is because the brittle nature of the new materials makes them susceptible to localized stress concentrations, which means that bond characteristics of these materials are particularly important. It is concluded that the choice of an appropriate analysis technique depends on the amount of debonding that FRPs are able to undergo during shear collapse of the concrete structure.

Keywords: fiber-reinforced plastics; finite element analysis; reinforced concrete; shear strength.

INTRODUCTION

To combat the corrosion of steel reinforcement in concrete structures, there are many options open to the engineer during the design phase. Uses of stainless steel, including cathodic protection methods, epoxy coatings, galvanizing, or other specifications, may all be considered. Alternatively, the use of steel reinforcement may be abandoned altogether. The use of fiber-reinforced plastics (FRPs) is now being considered for reinforcement of concrete structures.[1] These fibers hold a number of advantages over steel. First, they do not corrode. Second, they are lighter than steel, which is convenient for handling during construction. Third, they exhibit an ultimate tensile strength greater than that of either reinforcing or prestressing steel. Finally, the amount of concrete cover needed to protect FRPs is reduced, leading to lighter structures overall.

Drawbacks of these materials include purely elastic, brittle behavior under increasing load. Further, FRPs have lower stiffnesses than steel; larger structural deformations may be expected. Currently, FRPs are expensive and, importantly, cannot be easily bent into shapes or otherwise manipulated on site.

Some work has been conducted on the shear capacity of concrete reinforced with FRPs.[1,2] This work has been aimed specifically at determining the modifications that would need to be made to existing codes of practice to ensure that designs using such materials would be safe. While such work is desperately needed, the question arises as to whether or not the FRPs are being used as efficiently as possible.[3]

As a first step in attempting to answer this question, it was considered necessary to conduct a series of pushoff tests on concrete shear blocks reinforced with steel stirrups,[4] glass fiber-reinforced plastic (GFRP) stirrups, or aramid fiber-reinforced plastic (AFRP) helixes.[5] The results from such testing are discussed in terms of shear resistance, ductility, and bond, and compared with applicable theoretical models.

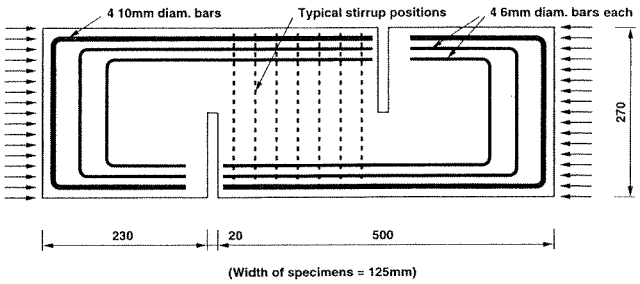

Fig. 1—Schematic view of shear-block specimens used throughout all testing.

RESEARCH SIGNIFICANCE

If the use of FRPs for the reinforcement of concrete structures is to become widespread, and subsequently attractive economically, these materials must be employed efficiently in any design. Therefore, a fundamental understanding of the behavior of concrete containing these materials is vital. Because these advanced composites are brittle, existing shear analysis techniques (based on relatively ductile steel-reinforced concrete) are probably inapplicable. A shear analysis tool for concrete containing these brittle materials that allows for the different variables that affect behavior is needed. Such an approach would lead to efficient design with FRPs.

EXPERIMENTAL PROGRAM

Pushoff shear tests

Mattock[6] carried out several pushoff tests on concrete shear blocks to obtain the relationship between the shear and normal stress acting along slip planes in steel-reinforced concrete structures. A similar approach has been adopted herein.

Figure 1 shows a schematic view of the shear blocks used throughout all testing. Where conventional stirrups were used as the shear reinforcement, these were fixed around the outside of the secondary reinforcement cages. Where the aramid helixes were used, these were fixed in the mold with the central helix crossing the shear plane and two outer intersecting helixes wrapped around the secondary reinforcement cages (Fig. 2). To inject ductility into a concrete structure containing brittle FRP reinforcement, one option is to use helical reinforcement in the compression regions.[3] Such helical reinforcement could also contribute to shear strength of the concrete. This effect is studied herein.

The target compressive cube strength of the concrete was 60 MPa when tested at 7 days. The steel stirrups of diameter 4 or 6 mm were found to have a yield strength of 382 or 393 MPa, respectively. The GFRP stirrups, of cross-sectional area 20 mm^2

ACI Structural Journal, V. 96, No. 6, November-December 1999.
Received June 29, 1998, and reviewed under Institute publication policies.

Tim Ibell *received his PhD from the University of Cambridge, England, in 1992. He is currently a lecturer at the University of Bath, England. His research interests include the use of advanced composites for the reinforcement of concrete.*

ACI member **Chris Burgoyne** *is a lecturer at the University of Cambridge. He is a member of ACI Committee 440, Fiber Reinforced Polymer Reinforcement. His research interests include advanced composites applied to concrete structures.*

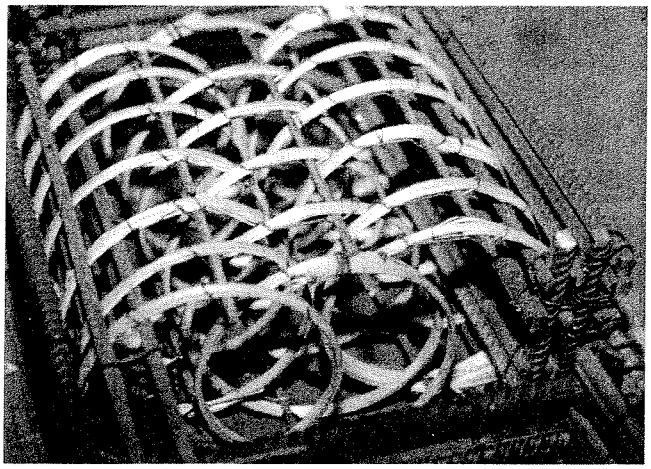

Fig. 2—Helical reinforcement positioning within mold.

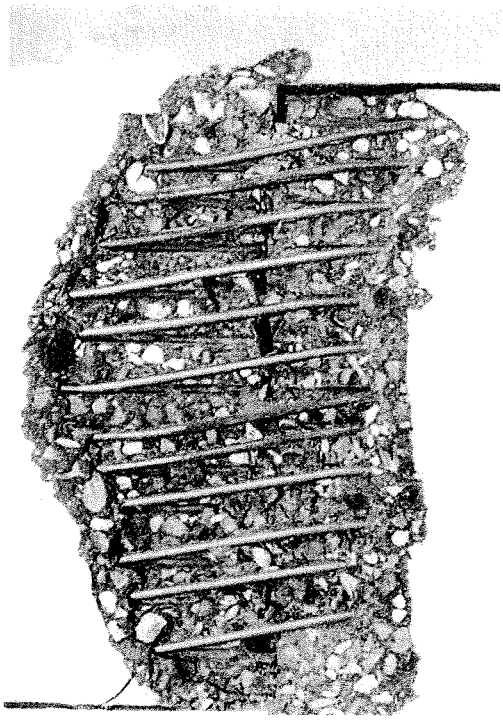

Fig. 3—Final collapse state of 1% steel-reinforced specimen.

Table 1—Test results for unreinforced specimens, and comparisons with elastic finite element predictions for shear capacity

Specimen no.	f_{cu}, MPa	f_t, MPa	Actual failure load, kN	Predicted failure load, kN
1	58.8	4.55	159	164
2	68.2	4.30	155	155

exhibited an ultimate strength of 425 MPa, with a Young's modulus of just 4 GPa. The AFRP helixes, of cross-sectional area 10 mm^2 had an ultimate tensile capacity of 1430 MPa. Young's modulus for the AFRP yarns was found to be approximately 120 GPa.

Results from unreinforced shear blocks

As a benchmark for all tests, two unreinforced specimens were tested initially. A catastrophic and exceptionally brittle failure was encountered in both cases. Table 1 shows details of the results obtained. In the same table are predictions from a linear elastic finite element analysis, assuming that when the tensile capacity of the concrete is exceeded at any point, collapse occurs. The agreement between results and theory is good.

Results from steel-reinforced shear blocks

These tests proved to be initially brittle, followed by a ductile, plastic, energy-dissipating period thereafter. Much cracking preceded the ultimate capacity being reached. Of the four tests conducted with steel stirrups, initial cracking along the central plane occurred at approximately 2/3 of the ultimate load on average. In addition, these initial cracks were oriented at approximately 15 C to the vertical, which agreed well with elastic finite element predictions. The concrete struts between these cracks were observed to rotate during subsequent loading, as might be expected.

Table 2 provides details of the steel reinforcement and failure capacity for each specimen. Figure 3 shows a close-up of the ultimate state of the second steel-reinforced specimen (with 1% shear steel). Note the spalled concrete and kinking of the steel bars across the central crack. In every test, all steel bars yielded

Table 2—Test results for steel-reinforced specimens

Specimen no.	f_{cu}, MPa	f_t, MPa	Steel shear stirrups	% area of stirrups	f_y, MPa	Actual failure load, kN
3	58.7	4.06	6 4 mm diameter	0.5	382	260
4	70.8	3.95	12 4 mm diameter	1.0	382	345
5	50.4	3.34	8 6 mm diameter	1.5	393	408
6	62.6	4.01	11 6 mm diameter	2.0	393	420

(strain gages were attached to the stirrups), reflecting the reasonably ductile response of these specimens. It should be noted, however, that, although prolonged crushing of concrete occurred along the central plane in a ductile manner, the ultimate capacity was reached at a vertical displacement of approximately 2 to 3 mm in each case. Beyond this displacement, the sustainable load dropped off gradually. Figure 4 shows details of these load-displacement plots.

Results from GFRP-reinforced shear blocks

A somewhat more brittle failure occurred in each case when reinforced with GFRP. Once the vertical displacement exceeded approximately 2 to 3 mm, however, the specimens exhibited ductility the same way as the steel-reinforced specimens, which was unexpected. Table 3 shows details of the stirrup reinforcement and failure capacities, while Fig. 5 shows the ultimate state of the second specimen (with 1% reinforcement). This form of failure is not dissimilar to that of the steel-reinforced specimens and shows that a long section of the GFRP stirrups has become unbonded. It is this spalling and debonding that caused local high strains in the GFRP to be spread over a longer section, reducing such strains (and hence stresses) and allowing some ductility to be displayed. Figure 6 shows the load-displacement plot for each specimen with GFRP stirrups. These plots highlight the initial peak load behavior, followed by a plateau-like zone at a lower load. Increasing

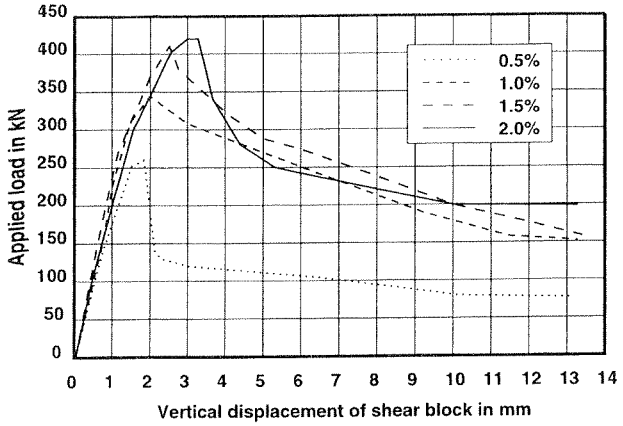

Fig. 4—Sustained load versus vertical displacement of shear blocks for all steel-reinforced tests.

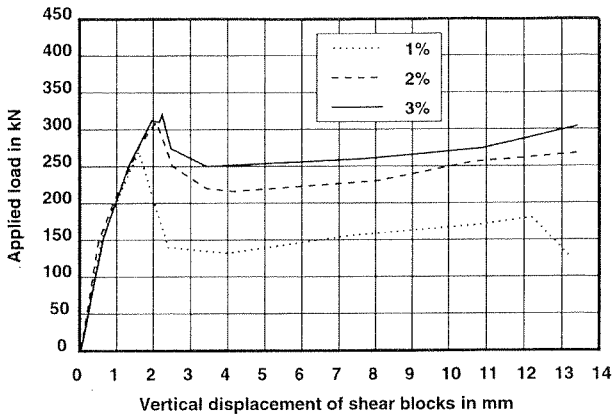

Fig. 6—Sustained load versus vertical displacement of shear blocks for all GFRP-reinforced tests.

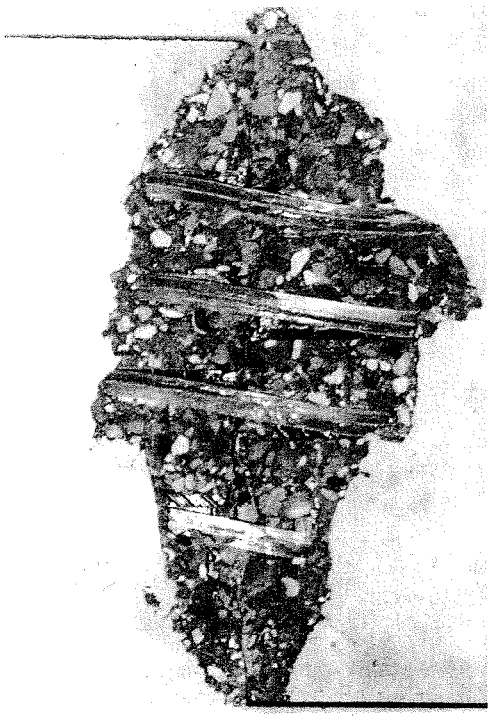

Fig. 5—Final collapse state of 1% GFRP-reinforced specimen.

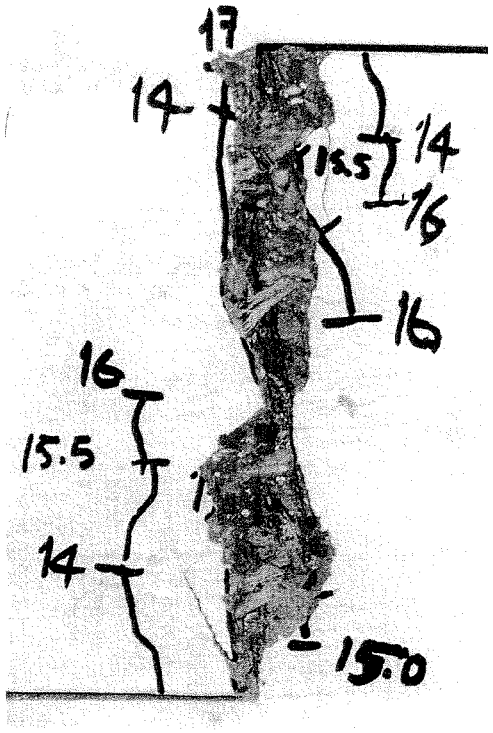

Fig. 7—Final collapse state of 7-leg AFRP helically-reinforced specimen.

Table 3—Test results for GFRP-reinforced specimens

Specimen no.	f_{cu}, MPa	f_t, MPa	GFRP shear stirrups	% area of stirrups	Actual failure load, kN
7	68.2	4.30	8 stirrups	1.0	270
8	67.2	4.30	16 stirrups	2.0	310
9	67.8	4.30	24 stirrups	3.0	330

carrying capacity occurred beyond this after the debonded length had reached a maximum, and the stirrup stress could gradually increase elastically until delamination of the stirrups caused abrupt failure.

Results from AFRP-reinforced shear blocks

An initially brittle form of failure was encountered for each of the helically AFRP-reinforced shear block specimens. Once again, however, marginal ductility (in the form of a plateau on the load-deflection curve) was observed beyond a displacement of approximately 2 mm and after the maximum load had been reached. Table 4 shows details of these test results, while Fig. 7 shows the ultimate state of the 7-leg helically reinforced specimen. Several points are immediately apparent.

The ultimate strength of the specimens is not affected as greatly by the presence of an increasing quantity of reinforcing material, as was the case for the GFRP reinforced specimens. It is thought that this is largely due to the helical arrangement not being able to debond after initial cracking, leading to localized stress concentration and premature snapping of the AFRP helixes. This is borne out by observation, where the limited spalling (Fig. 7) reflects such behavior. Further, the helixes seemed to snap at points where they had been tied (using thin steel wire) to the secondary reinforcement. It seems that the localized nature of debonding and stress concentration led to failure.

Figure 8 shows the load-displacement plot for each AFRP-reinforced specimen. It is clear from this plot that while some post-peak ductility is displayed, the previous results using GFRP (where debonding occurred over a longer section) are more desirable to a designer, both from ultimate strength and behavioral standpoints. It is not implied that one material is

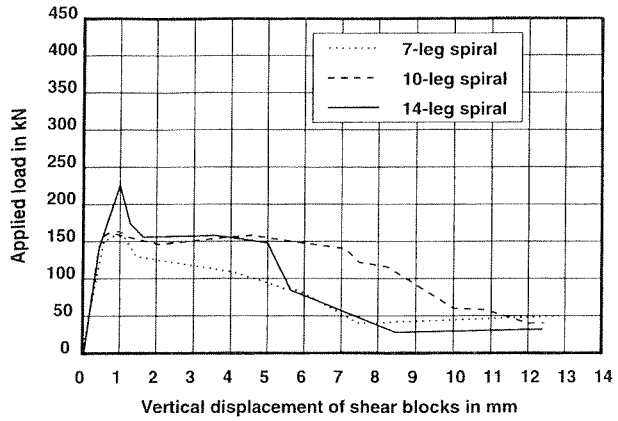

Fig. 8—Sustained load versus vertical displacement of shear blocks for all AFRP helically-reinforced tests.

Table 4—Test results for AFRP helically-reinforced specimens

Specimen no.	f_{cu}, MPa	f_t, MPa	AFRP helical windings	Actual failure load, kN
10	49.7	3.40	7 legs	170
11	65.1	3.60	10 legs	165
12	49.7	3.40	14 legs	225

superior to another for the shear reinforcement of concrete, but rather that it is the geometry and bond characteristics of the material that influence both strength and behavior in shear.

SHEAR ANALYSIS TECHNIQUES

Plasticity theory applied to steel-reinforced specimens

An analytical tool is sought to predict the ultimate strength in shear of concrete reinforced with various materials. One option is the use of upper-bound plasticity theory. Due to the relatively brittle nature of collapse of the FRP-reinforced specimens, however, plasticity theory will only be applied to the steel-reinforced specimens, where comparatively more ductility was displayed.

The following assumptions are made regarding the use of plasticity theory applied to concrete:

1. Rigid perfectly plastic collapse occurs with all failing material developing full strength. Elastic deformations are negligible.

2. The Modified Coulomb failure criterion with nonzero tension cutoff is assumed for the concrete.[7] The internal angle of friction ϕ is assumed to be a constant 37 C for all combinations of stress. In separation failures, a limiting tensile strength of concrete f_t is assumed, where applicable, but $f_t = 0$ in this case.

3. The shear blocks are acting under conditions of plane strain (so that the relative displacement angle between rigid blocks α is greater than or equal to ϕ in all cases.)[7]

4. The steel bars carry axial tension forces only. Any dowel effects are ignored, in accordance with standard concrete plasticity.

5. Effectiveness factor ν is applied to the compressive strength of the concrete to allow for lack of ductility in plain concrete and other effects.[7]

The model consists of an S-shaped line of discontinuity (Fig. 9) along the central axis of each specimen, a shape that was observed to form to a greater or lesser extent throughout all tests. The S-shape consists of two identical circular arcs. The radius of these arcs is considered a variable. Block 1 moves relative to Block 2 without rotation. Therefore, the notional relative displacement between each block is constant along the entire length of discontinuity. This relative displacement is restricted

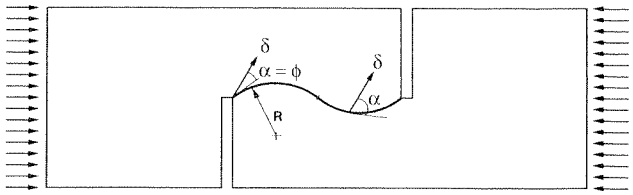

Fig. 9—General form of shear failure geometry in shear blocks.

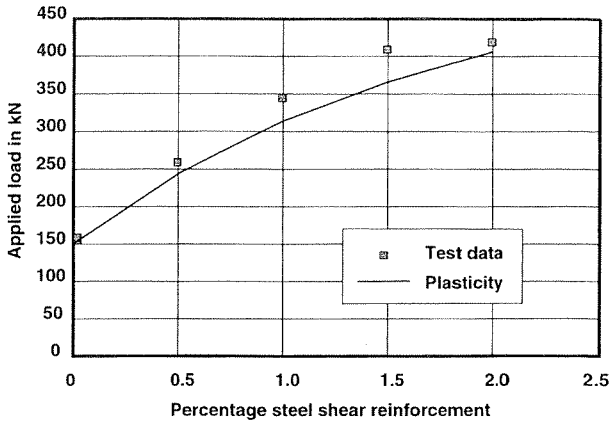

Fig. 10—Plot of predicted and actual shear capacities for steel-reinforced specimens, for increasing percentages of reinforcement.

to be an angle α, which is equal to ϕ (37 C) at the top and bottom of the failure surface, where α is a minimum by inspection. Elsewhere, $\alpha \geq \phi$, which satisfies the third assumption that the shear block is in a state of plane strain.

The energy dissipation rate along the length of the discontinuity is calculated according to the following simple equation, derived elsewhere[7]

$$\dot{D} = \frac{1}{2}\delta f_c b(1 - \sin a) \quad (1)$$

where δ is the notional relative displacement between the two rigid portions, f_c is the effective strength of concrete ($= \nu f_{cu}$), b is the breadth of specimen, and a is the angle between the line of discontinuity (at any point) and the relative displacement vector δ.

The energy dissipation in the concrete is integrated numerically along the curved line of discontinuity. The energy involved in stretching each steel bar that crosses the central line of discontinuity is calculated as the steel yield force in each bar multiplied by the notional distance through which it is stretched axially. This energy is added to the concrete energy contribution to find the total internal energy dissipation. The external work done on the shear block due to the load P is found by multiplying P by the notional vertical distance through which it has moved, and is compared with the internal energy dissipation. The radius of the two arcs is then altered slightly in a logical progression, and the process is repeated until the optimum shape of the failure surface is found such that the ratio between internal energy dissipation and external work done is a minimum. This minimum load factor corresponds to the lowest upper-bound estimate of the shear strength of the specimen.

Using this approach, Fig. 10 shows a plot of the predicted ultimate capacity of each steel-reinforced specimen compared with the actual test data. A value for the effectiveness factor of 0.50 has been assumed for the concrete. Many values for the effectiveness factor for shear in concrete have been suggested,[7] but a midrange

Table 5—Predicted capacities versus actual test results for GFRP-reinforced specimens

Specimen no.	Minimum actual sustained load, kN	Predicted sustained load, kN
7	135	150
8	215	200
9	250	240

value has been adopted herein. There appears to be reasonably good correlation between theory and reality in this case.

Analysis of GFRP-reinforced specimens

It seems nonsensical to apply the theory of plasticity (shown to model the steel-reinforced specimens well) to the GFRP-reinforced specimens. A different approach is required, due to lack of yielding and plastic dissipation possible in the GFRP stirrups themselves.

Therefore, an analysis based on the work of Walraven[8] is conducted for these specimens. Walraven developed expressions for the relationship between normal stress, shear stress, shear slip, and width across a crack in concrete. His theory is based on tests conducted on precracked concrete pushoff tests, so that the initial peak strength of the concrete blocks in the present work cannot be modeled using this approach. It is the postpeak plateau-like region that is of interest to the designer if a safe design is to result from using these brittle materials.

The analysis conducted consists of the following:

1. A bond strength of the GFRP material is assumed. A bond strength σ_{bond} of 16 MPa has been assumed in these analyses. This value is quite high, but comparable with strengths observed in tests by various authors, including Lees,[9] though the bond strengths of FRPs are very variable and dependent on many factors.

2. From test results, it appears that the width of the crack when plateau-like behavior was initiated was approximately 0.5 mm. Therefore, a crack width w of 0.5 mm in the analysis is assumed.

3. From the assumed bond strength of the material and crack width, an expression is written down for the debonding length l_{debond} of the GFRP stirrups across the crack as

$$l_{debond} = \frac{\frac{2F_{leg}}{2}}{\sigma_{bond} \cdot l_{perim}} \tag{2}$$

where F_{leg} is the maximum force in each stirrup leg (assuming that each stirrup carries an equal portion of the load) and l_{perim} is the perimeter of the GFRP stirrup leg cross section. Note that the force in each leg is assumed to vary linearly from a maximum of F_{leg} at the crack to zero at a distance $l_{debond}/2$ to either side of the crack.

4. The crack width w is then

$$w = \frac{\frac{F_{leg}}{2} \cdot l_{debond}}{A \cdot E} \tag{3}$$

where A is the cross-sectional area of the GFRP leg and E is Young's modulus for GFRP.

5. The maximum force in each stirrup leg may then be evaluated by combining Eq. (2) and (3)

$$F_{leg} = \sqrt{(2 \cdot w \cdot \sigma_{bond} \cdot l_{perim} \cdot A \cdot E)} \tag{4}$$

6. The normal stress in the concrete across the crack due to this force is calculated as

$$\sigma = \frac{F_{leg} \cdot n \cdot 2}{b \cdot h} \tag{5}$$

where n is the number of stirrups present, b is the breadth of the block, and h is the length of the central shear crack.

7. Then, using Walraven's analysis, the shear stress τ and shear slip Δ associated with the above normal stress σ, and crack width w may be evaluated.

8. The predicted capacity P of the blocks can then be calculated from

$$P = \tau \cdot b \cdot h \tag{6}$$

Using this analysis procedure, Table 5 shows the predicted sustained capacities of the GFRP-reinforced shear blocks, after the initial peak strength has been reached. These strength values compare favorably with the minimum sustained load in the postpeak plateau region $P_{plateau}$ for each test.

Analysis of AFRP-reinforced specimens

These specimens contained helixes of small diameter that would have been very highly stressed at localized points. Indeed, snapping of these helixes occurred at relatively low load. It seems inappropriate, therefore, to conduct an analysis of the concrete when failure of these specimens was due largely to rupture of the helixes themselves. In turn, this rupture appears to have been initiated at tying points of the helixes, where stress concentrations would have been worst.

Therefore, it seems most sensible to conduct an analysis of the structure that assumes it is entirely elastic and that full bond exists between AFRP and concrete. In this way, an idea of the stresses present in the AFRP may be found.

A linear elastic finite element (FE) analysis was conducted on such a specimen. The results show that the central zone of the block has the highest transverse tensile stress. This tensile stress σ_{tmax} has magnitude (in N/mm^2)

$$\sigma_{tmax} = 0.0278P \tag{7}$$

where P is the applied load in kN.

After initial cracking has occurred, it was postulated that the full elastic tensile stress that was present in the concrete prior to cracking is wholly transferred to the nearest bonded AFRP helical leg. Therefore, the central leg will need to be able to carry a load

$$F_{leg} = \frac{0.0278P \cdot b \cdot h}{n} \tag{8}$$

where n is the number of helical legs present. Given that the observed strength of a single leg (as measured in a separate test) $F_{leg} = 14.3$ kN from initial tests, $b = 125$ mm, and $h = 250$ mm, the following predicted loads at which the central leg becomes overstressed (assuming perfect bond) are:

7-leg helixes: $P = 115$ kN
10-leg helixes: $P = 164$ kN
14-leg helixes: $P = 230$ kN

The predicted load for the 7-leg helix is below the cracking load for the unreinforced equivalent specimen (122 kN for $f_t = 3.40$ MPa). Therefore, the prediction for the 7-leg helically-reinforced specimen is a minimum of 122 kN. Table 6 shows comparisons between actual test results and these simplified

Table 6—Predicted capacities versus actual test results for AFRP helically-reinforced specimens

Specimen no.	Actual failure load, kN	Predicted failure load, kN
10	170	122
11	165	164
12	225	230

analyses. The agreement is good once again, except for Specimen 10, where the prediction is poor. A possible explanation for this could be that the fiber initially carries some of the load, so that Specimen 10's strength exceeds that of the concrete acting by itself. Once the concrete has failed, the maximum strength of the specimen is governed by the strength of the fiber acting alone (which happened with the two more heavily-reinforced specimens). More tests would be needed to determine whether this was, indeed, the case. Note that an implicit assumption is made that when the helix snaps at any point; failure occurs by unraveling of the helix thereafter. This was observed, with the entire specimens seen to twist in plan after initial snapping of the AFRP had occurred.

CONCLUSIONS

The use of aramid helixes, instead of the stirrups used for the glass-reinforced links, was imposed by the availability of material. It fortuitously shows, however, that the idea that shear strength can be based solely on the amount of reinforcement, and its strength, which is the basis of design with steel links, is wholly inappropriate for specimens with FRP links. Instead, the geometry of the links and their bond characteristics are much more important.

The following detailed conclusions may be drawn:

1. Steel-reinforced shear block specimens failed along a clearly defined discontinuity, initially in a brittle manner, but thereafter with some plastic deformation in a controlled manner.

2. GFRP-reinforced specimens failed in a somewhat more brittle manner, although some plasticity was observed during postpeak behavior. The debonding of the GFRP stirrups was a particularly important observation. This debonding allowed substantial deformation of the structure (and stirrups themselves) to occur prior to delamination of the GFRP.

3. AFRP helically-reinforced specimens failed in a very brittle manner. In fact, failure was due to snapping of the AFRP at relatively low load. This was most likely due to the helixes being tightly wound, so that there was little chance of debonding. Stress concentrations would have built up and caused rupture. This was perhaps exacerbated by tying-wires, at the locations at which rupture usually occurred.

4. An upper-bound plasticity approach has been shown to adequately model the behavior of the steel-reinforced specimens. Conversely, it is suggested that plasticity theory should not be applied to the FRP-reinforced specimens where the constituent reinforcing materials exhibit no plastic energy dissipation during stretching to failure.

5. An analysis using Walraven's approach was applied to the GFRP-reinforced specimens. Reasonably accurate predictions were obtained for the postpeak sustainable strength of these specimens.

6. Analysis of the AFRP helically-reinforced specimens is more problematic due to the premature nature of failures, caused by local stress concentrations due to high bond strengths. A simplified elastic finite element analysis shows that the central leg of the helix becomes overstressed in each case (if full bond is assumed between concrete and AFRP), leading to snapping, unraveling of the helix, and dramatic failure.

7. The strength of these three sets of specimens cannot be determined on the basis of the strength of the reinforcement, or the strength of the concrete alone. The geometry of the reinforcement, and whether or not it can debond, and if so, over what length, is at least as important. It thus follows that no simple analysis based on plasticity theory, even with the addition of a strain limit, can describe the behavior of sections reinforced with FRPs.

NOTATIONS

A = cross-sectional area of one leg of GFRP stirrup, mm^2
b = breadth of test specimens (125 mm)
D = energy dissipation rate per unit length of shear discontinuity
E = Young's modulus for steel, GPa
F_{leg} = maximum force in GFRP stirrup leg, kN
f_c = effective strength of concrete, MPa
f_{cu} = compressive cube strength of concrete, MPa
f_t = split-tensile strength of concrete, MPa
h = length of shear plane in specimens (250 mm)
l_{debond} = length over which debonding of GFRP occurs, mm
l_{perim} = perimeter of section of GFRP stirrups, mm
n = number of stirrups or number of helical windings
w = width of shear crack, mm
P = load applied to specimen, kN
$P_{plateau}$ = minimum sustained load in postpeak region, kN
α = angle between δ and shear discontinuity, rad
Δ = shear slip along shear plane, mm
δ = relative displacement vector between two rigid blocks
ϕ = internal angle of friction for concrete (37 degrees)
ν = effectiveness factor for concrete strength
σ = normal stress in concrete, MPa
σ_{bond} = bond stress between GFRP and concrete, MPa
σ_{tmax} = maximum transverse tensile stress in concrete, MPa
τ = shear stress in concrete, MPa

ACKNOWLEDGMENTS

These tests were conducted at Cambridge University Engineering Department by M. A. El-Hassan and M. Rich. Their participation in this research is gratefully acknowledged, as is the technical help provided by C. J. Mason, V. L. Piper, and M. R. Touhey.

REFERENCES

1. Clarke, J. L., and Waldron, P., "The Reinforcement of Concrete Structures with Advanced Composites," *The Structural Engineer*, V. 74, No. 17, Sept. 1996, pp. 283-288.

2. Tottori, S., and Wakui, H., "Shear Capacity of RC and PC Beams Using FRP Reinforcement," *Proceedings of FRP Reinforcement for Concrete Structures*, Vancouver, Mar. 1993, pp. 615-632.

3. Burgoyne, C. J., "Rational Use of Advanced Composites in Concrete," *Technical Report*, CUED/D-Struct/TR167, Cambridge University Engineering Dept., 1997.

4. Elhassan, M. A., "The Coefficient of Friction in Concrete," final year project report, Cambridge University Engineering Dept., 1991.

5. Rich, M., "Shear in Concrete Reinforced with Fibre-Reinforced Plastics," final year project report, Cambridge University Engineering Dept., 1996.

6. Hofbeck, J. A.; Ibrahim, I. O.; and Mattock, A. H., "Shear Transfer in Reinforced Concrete," ACI JOURNAL, *Proceedings* V. 66, No. 2, Feb. 1969, pp. 119-128.

7. Nielsen, M. P., *Limit Analysis and Concrete Plasticity*, Prentice-Hall, 1984.

8. Walraven, J. C., "Fundamental Analysis of Aggregate Interlock," *Journal of the Structural Division*, ASCE, V. 107, No. 11, Nov. 1981, pp. 2245-2270.

9. Lees, J. M., and Burgoyne, C. J., "Bond Characteristics of FRP Reinforcement." (submitted to *Magazine of Concrete Research* for publication)